Elastic and inelastic scattering of ^{12}C by ^{12}C from $E_{c.m.} = 35$–63 MeV

R. G. Stokstad, R. M. Wieland, G. R. Satchler, C. B. Fulmer, D. C. Hensley, S. Raman, L. D. Rickertsen, A. H. Snell, and P. H. Stelson

Oak Ridge National Laboratory, Oak Ridge, Tennessee 37830

(Received 19 March 1979)

Differential cross sections for the elastic scattering, single excitation ($Q = -4.43$ MeV), and mutual excitation ($Q = -8.86$ MeV) of ^{12}C by ^{12}C have been measured at 14 bombarding energies in the range $E_{c.m.} = 35$–63 MeV. The angular distributions extend typically from 16° to 90° c.m. The results have been analyzed with the optical model, the distorted-wave approximation, and the method of coupled equations. The optical model analysis of the elastic scattering reveals a sensitivity of the predicted cross sections at large angles to the strength and shape of the real part of the nuclear potential in the region 4 to 6 fm. The potentials predicted by the double-folding model fit the data remarkably well over the entire angular range, whereas the shallow potentials which we have explored generally fit the data only in the forward-angle region. The results thus indicate that the real potential for the $^{12}C + ^{12}C$ system is more attractive in the region of 4 to 6 fm than would have been expected on the basis of previous analyses of comparable systems at lower bombarding energies.

[NUCLEAR REACTIONS $^{12}C(^{12}C, ^{12}C)$, $E_{c.m.} = 35$–63 MeV; measured $\sigma(E, \theta)$ for elastic, single, and mutual excitation of 2^+. Optical model, DWBA analyses.]

I. INTRODUCTION

Generally, the dominant physical process governing the elastic scattering of heavy ions is that of strong absorption. The features of strong absorption, as embodied in the models of Blair,[1] McIntyre *et al.*,[2] and Frahn and Ventner[3] are sufficient to explain many of the gross characteristics of elastic and inelastic scattering as observed for complex nuclear systems throughout the periodic table. Within this framework the scattering is determined only by the surface regions of the colliding nuclei, with the interior region remaining black and inaccessible.[4] This has sometimes been obscured by the arbitrary choice of a Woods-Saxon form factor to describe the real potential and the concomitant parameterization in terms of a central depth, as well as a radius and a diffusivity. Consequently it has proven necessary to reemphasize through various quantitative procedures the inherent blackness of the nuclear interior.[5,6]

The nuclear surface, however, has provided a fruitful area of investigation. It has been possible to study in detail the transparency of the nuclear surface[7-9] and its collective motion, to suggest the existence of nuclear orbiting or shape resonances,[7,9,10] and to predict the effects of coupling to excited states.[11] Part of the fascination of systems with projectiles and targets in the mass range $A = 12$–20 has been the appearance of pronounced gross structure in the excitation functions.[7,9,10] These structures have their origin in the concept of strong absorption—like the angular oscillations, they are diffractive in nature—but they owe their varying intensity in different scattering systems to the details of the particular nuclear surfaces and to the types of reactions which occur at the surface. A recent review of this area has been given by Siemssen.[9]

Since the bulk of the interactions which are responsible for strong absorption leads to compound nucleus formation (at least at energies $\lesssim 15$ MeV/A), there is the possibility that compound nucleus decay will also contribute significantly to the elastic scattering. This contribution is calculable on an averaged basis, but its detailed nature cannot be predicted by theory. In systems such as $^{12}C + ^{12}C$ at lower energies, where the number of open channels is relatively small, compound elastic scattering is an important effect.[12,13] This and the fact that the diffractive aspects of the scattering result in cross sections which vary rapidly with energy and angle require that experimental data covering a wide range of energy and angle be available for analysis. Such data have been available for $^{12}C + ^{12}C$ at energies below 30 MeV c.m.,[14-17] but above this energy there exist only the measurements of Wang *et al.*[18] and Garvey *et al.*[19] at 60 MeV c.m. and which extend only to $\theta_{c.m.} \lesssim 45°$. Recent experiments with $^{16}O + ^{16}O$ (Ref. 20) and $^{12}C + ^{12}C$ (Ref. 21) in which an excitation function at 90° c.m. has been measured have shown that the gross structure observed at lower energies persists in this higher energy region.

We have undertaken to measure complete angular distributions in this relatively unexplored region and have done so at 14 bombarding energies over the range 30–63 MeV c.m. At these high bombard-

ing energies, the contributions of compound elastic scattering are predicted to be much smaller than at lower energies, thus enabling an analysis of angular distributions at individual energies instead of energy-averaged excitation functions. We find that the optical model accounts very well for the observed features of the elastic scattering and that the distorted-wave approximation (DWA) and coupled equations analysis allow an understanding of the inelastic scattering in terms of the collective model. The main result of our analysis of this rather large body of data is that our knowledge of the nuclear potential has been extended about 2 fm further inward by measurements of the differential cross section at high energies and at large scattering angles. The nuclear potential in this interior region now appears deeper than previously supposed. A portion of the analysis of the elastic scattering has been published previously.[22]

II. EXPERIMENT

Differential cross sections for the elastic and inelastic scattering of ^{12}C by ^{12}C have been measured over a wide range of bombarding energies from $E_{1ab} = 70.7$ to 126.7 MeV. Differential cross sections for one- and two-nucleon transfer were also measured at one energy, $E_{1ab} = 93.8$ MeV, and are described in Ref. 23. A complete tabulation and graphical representation of all the experimental data are available on request.[24]

Different experimental arrangements were used at different times. In the first experiment, data were taken at $E_{1ab} = 74.2$, 83.3, 89.7, 98.2, 102.1, 106.9, and 117.1 MeV, with the apparatus illustrated schematically in Fig. 1. The angular distributions were measured using a solid-state, position-sensitive detector (PSD) covered by a mask containing 15 apertures, each 1.59 mm wide × 11.4 mm high. The apertures, placed at a distance of 18 cm from the target, were thus spaced 1° apart and subtended an angular opening of $\frac{1}{2}$° each. The range from 11° to 47° (lab) was covered with three separate settings of the PSD, with several apertures providing overlap points at each end of the mask. The inability of the PSD to resolve the mutual excitation of the first-excited states of the target and projectile ($Q = -8.88$ MeV) from the single excitation of the 3^- state ($Q = -9.64$ MeV) necessitated their separation by a kinematic-coincidence technique. (The 3^- state is unbound and therefore cannot produce a kinematic coincidence.) A large detector, 10 mm × 50 mm, was placed 9 cm from the target. Because the target contained no substantial amount of contaminants, it was not necessary that this detector be position sensitive, thus simplifying the apparatus and especially the data collection.

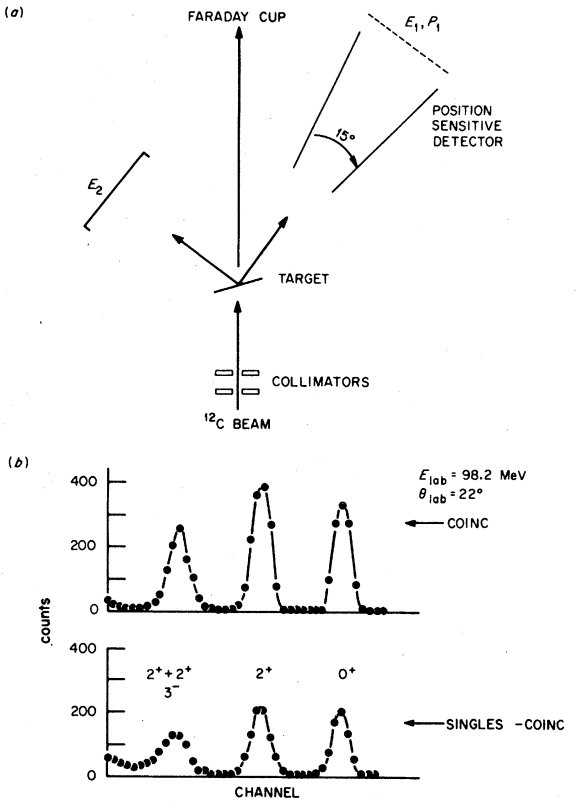

FIG. 1. (a) Schematic diagram of the experimental arrangement used for the kinematic-coincidence measurements. (b) A typical energy spectrum for one of the apertures; a coincidence with the recoil detector (E_2) has been required. The lower-spectrum shows those events for which there was no coincident particle of the appropriate energy in the E_2 detector.

The singles and coincidence data were stored in separate two-dimensional arrays. Each array consisted of 200 channels (position) by 200 channels (energy). Events were placed in either array according to whether a particle with the correct energy was observed in the conjugate detector.

The coincidence efficiency did not approach 100% because of the vertical height of the beam spot (about 6 mm). Except for the four most forward angles, however, the coincidence efficiencies as predicted by a geometrical calculation and determined empirically from the measured ratios of singles and coincidence events agreed very well. Thus this method provided a reasonably effective means for separating the mutal excitation from the excitation of the 3^- state at laboratory angles of 15° and greater.

The target thickness was about 50 $\mu g/cm^2$ and was effectively monitored for carbon buildup during the course of the measurements. Nevertheless,

the target thickness remained the largest source of error in the cross sections, which are estimated to have an absolute uncertainty of about ± 15%. The overall angular resolution and precision are estimated to be ± 0.6° (lab) and ± 0.15° (lab), respectively.

An angular distribution was subsequently obtained at $E_{lab} = 70.7$ MeV with the PSD as described above, but without the kinematic coincidence.

In the second experiment, a different type of PSD was used. It consisted of 25 individual detectors on a single silicon chip.[25] Each detector or "slice" was 14 mm in height and subtended an angular width of about 0.6°. This detector offered a much improved efficiency for data collection over the previous detector. Because the results obtained with the kinematic-coincidence apparatus indicated that the yield of the 3^- state is small, compared to that of the mutual excitation for laboratory angles $\gtrsim 15°$, the recoil detector was omitted. A substantially thicker target (~180 $\mu g/cm^2$) was used. Its thickness was determined by α-ranging measurements. The stopping power for α particles in carbon was determined by measuring the energy loss in thicker carbon foils (~300 $\mu g/cm^2$) whose thicknesses had been measured by weighing. The value used was $dE/dx = 0.693 \pm 0.028$ keV/$\mu g/cm^2$ for $E_\alpha = 5.75$ MeV. Angular distributions were measured at bombarding energies of 78.8, 93.8, 105.0, 112.0, 121.6, 117.1, and 126.7 MeV. The systematic error in the absolute normalization for these data is ± 13%.

A short experiment at 98.2 MeV was made using the broad-range spectrograph. This allowed the resolution of the mutual and 3^- excitation, and enabled measurement at more forward angles. A momentum spectrum is shown in Fig. 2.

III. RESULTS

The results are presented graphically in Figs. 3–5. Errors greater than 5% result from counting statistics, background subtraction, and, in the case of the kinematic-coincidence experiments, include a small contribution for the uncertainty in the coincidence efficiency in the determination of the mutual excitation ($Q = -8.86$). A minimum random error of 5% has been estimated, independent of counting statistics. All of the results have been normalized to the measurements made with the 180 $\mu g/cm^2$ carbon target. The adjustments made to the other angular distributions in renormalizing them were all less than 10%. Thus, the systematic error on the absolute normalization arising from target thickness, beam-current integration, and solid-angle measurement is conservatively estimated at ± 15% for all data.

For those angular distributions in which the contributions of the 3^- state at 9.64 MeV and the mutual excitation at 8.86 MeV are not distinguished

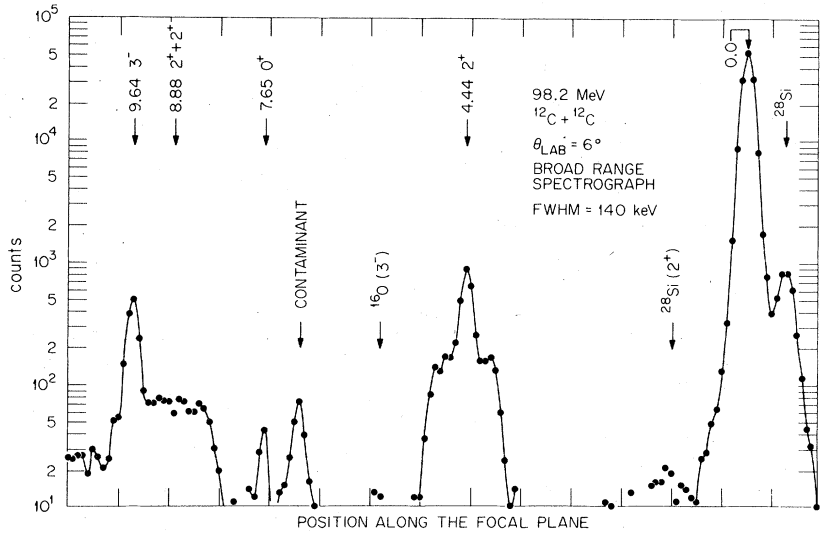

FIG. 2. A high-resolution spectrum taken at $\theta_{lab} = 6°$ and $E_{lab} = 98.2$ MeV with the broad-range spectrograph. The resolution was 140-keV fwhm for an angular acceptance of $\sim\frac{1}{2}°$. Note the interesting shape of the particle group corresponding to excitation of the 2^+ state. The narrow peak results from detection of the ^{12}C nucleus which was not excited to the 2^+ state. The broad peak corresponds to detection of the partner which was excited and experienced a change in energy and angle upon emission of a 4.43-MeV γ ray. The peak representing the mutual excitation is the superposition of two such Doppler-broadened groups. The excitation of the 3^- state is observed as a sharp group, since only the ^{12}C nucleus which remained in its ground state lives to be detected.

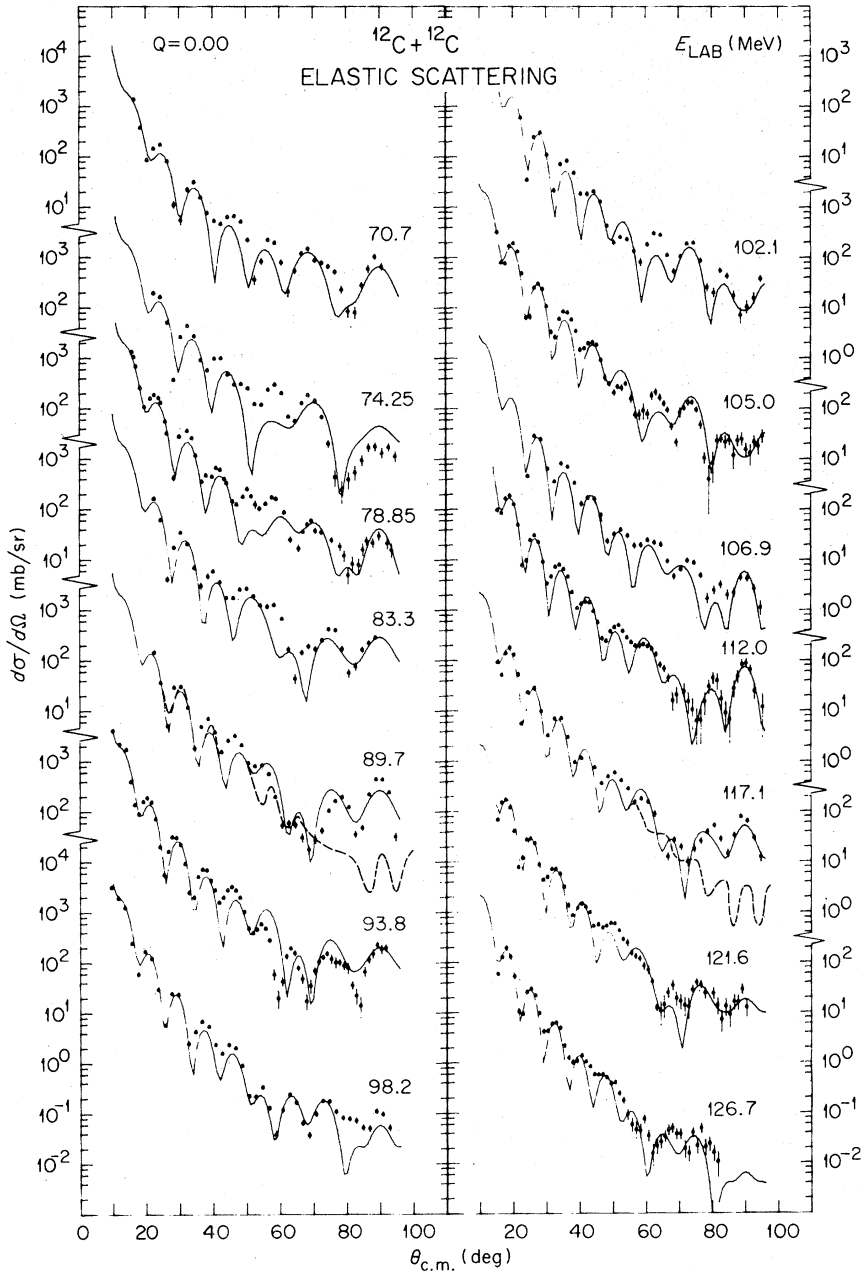

FIG. 3. The elastic scattering of ^{12}C by ^{12}C. The appropriate ordinate for each angular distribution is obtained by reading the cross section for the forwardmost angle of each angular distribution. The full curves are the results of optical model calculations described in the text.

the following observations hold: For c.m. angles larger than a value θ_c, the mutual excitation dominates, with the 3^- state contributing less than 7% of the counts in the peak. From measurements made with the kinematic-coincidence technique θ_c is estimated to decrease approximately linearly with bombarding energy from 53° c.m. at 71 MeV to 17° c.m. at 120 MeV. For angles in the range of 25–35° c.m. and bombarding energies below 100 MeV lab the 3^- contribution can be significant, in the range of 10–50%. At angles less than 20° c.m. the 3^- contribution probably dominates.

The cross sections have the following definition: For elastic scattering and for mutual excitation ($Q = -8.86$ MeV) the scattered particle and the recoil nucleus are indistinguishable, and the experi-

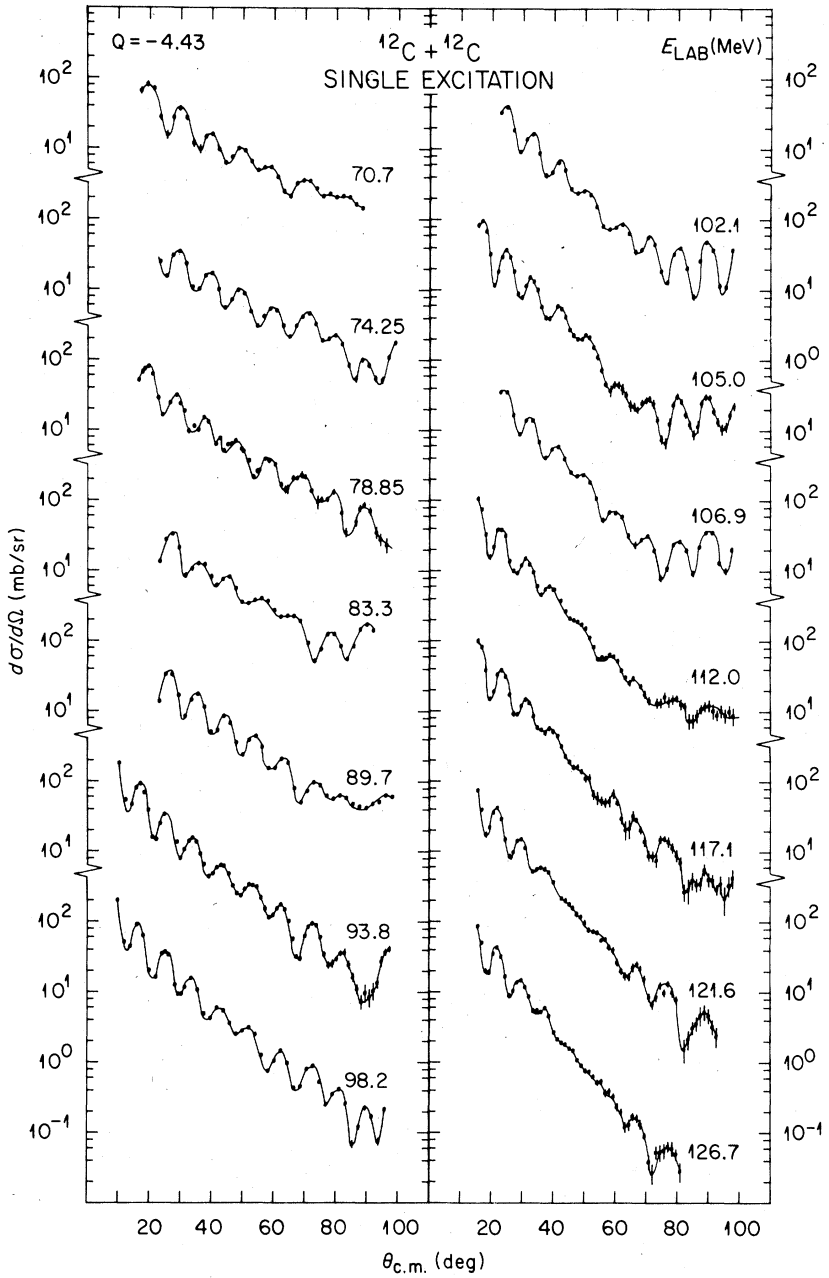

FIG. 4. The single excitation of ^{12}C by ^{12}C. See the text for the definition of the cross section. The ordinate is obtained in the same way as for Fig. 3. The full curves are only to guide the eye.

mental cross section includes the (equal) contributions from both the scattered particle and recoil nucleus. For single excitation ($Q = -4.43$ MeV) the residual ^{12}C nuclei are distinguishable because the excited nucleus emits a γ ray. In Figure 2 the effect of the small recoil energy imparted by γ-ray emission can be seen as introducing an energy-broadened component in the spectrum. The resolution of the solid state detector does not allow the observation of these two components. Hence all cross sections for single excitation include the (equal) contributions from the excited and the unexcited ^{12}C nuclei.

Figure 6 shows a two-dimensional representation of the elastic cross section as a function of bombarding energy and scattering angle. It is of interest to compare the regularity of the structure shown in this figure with a comparable representa-

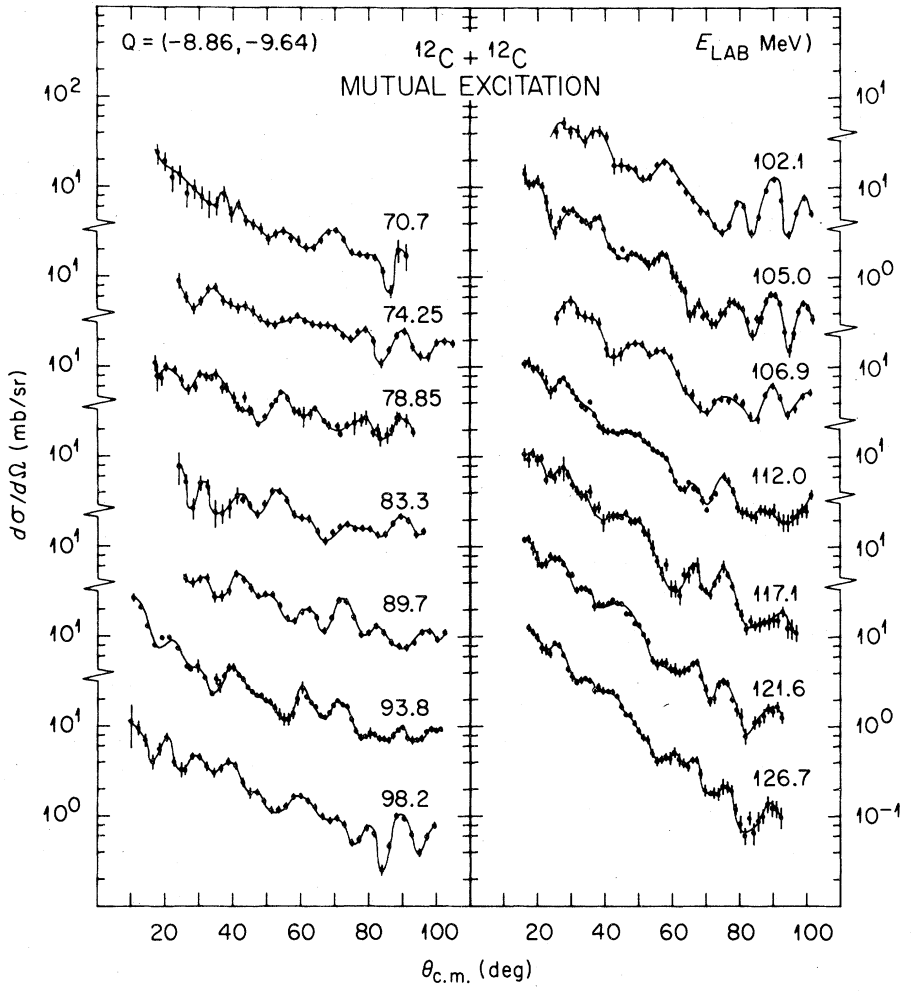

FIG. 5. The mutual excitation of ^{12}C by ^{12}C. See the text for the definition of the cross section and a discussion of the contribution of the 3^- state. The ordinate is obtained as in Fig. 3. The full curves are only to guide the eye.

tion in Ref. 16 (Fig. 9) for the elastic scattering observed at lower energies.

IV. ANALYSIS

A. Elastic scattering

Elastic scattering angular distributions were calculated with the optical model code HIGENOA,[26] using a number of real and imaginary Woods-Saxon potential forms with widely varying parameters. These calculated cross sections were compared with the measured angular distributions, and several sets of radius and diffuseness parameters (r_V, a_V, r_W, a_W) were obtained which seemed to describe best the data over the entire range of energies studied. With these geometrical parameters thus fixed, the depths of the real and imaginary potentials were allowed to vary in order to optimize the fit to the data at each energy.

This fitting procedure first emphasized the obtaining of good fits to the forward-angle data ($\theta_{c.m.} \lesssim 50°$), and only then were the more difficult backward-angle data ($50° \lesssim \theta_{c.m.} \lesssim 100°$) considered. The ultimate judgement of "goodness of fit" was left to the eye, reflecting the insensitivity of the χ square to small parameter variations which changed the nature of the fit at the most backward angles.

1. Woods-Saxon real potentials

Several families of Woods-Saxon potentials were investigated. They are listed in Table I, where the respective parameter ranges are indicated. Potential family *A* includes a series of very deep potentials which were designed to resemble the folded potentials which are discussed later in this section. The type *B* potentials are similar to those

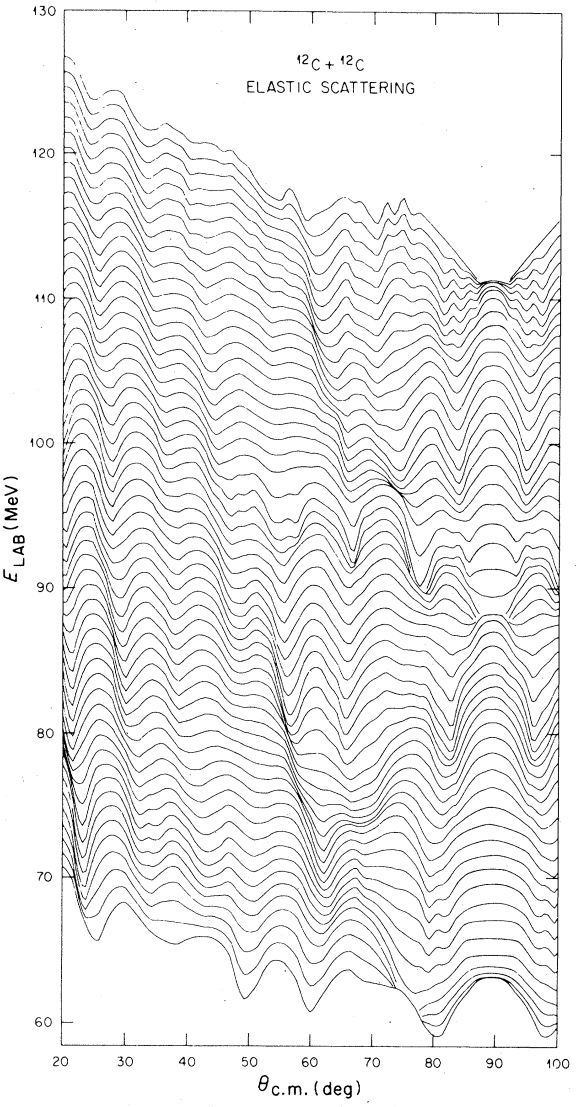

FIG. 6. Energy-angle plot of the differential cross section for elastic scattering. A two-dimensional logarithmic interpolation of the data has been made in order to plot the cross sections at 1 MeV (lab) intervals and as a continuous function of angle.

used by Reilly *et al.*[15] in their analysis of ^{12}C elastic scattering excitation function data at energies lower than those studied here. The type *C* potentials are of the type used by Gobbi *et al.*[7] in a similar analysis, where the imaginary radius was made smaller than the real radius, thus duplicating the improved fits found earlier[27] using an angular-momentum-dependent imaginary well depth.

None of the potentials appearing in Table I were able to reproduce the data at *both* forward and backward angles over the entire energy range under consideration here. They consistently underpredicted the backward-angle cross sections relative to the forward-angle data. Even when this was not the case for a particular energy the corresponding parameters were not successful in predicting the correct angular distribution at adjacent energies.

Finally, soft, repulsive cores[28] were introduced into the real potential, with no significant change in the quality of the fits.

2. *Folding-model potentials*

Folding-model real potentials have been used with good results in describing a number of heavy- and light-ion-induced elastic scattering measurements.[5,29] These potentials are given by the double-folding procedure,[5,29]

$$V(R) = \rho(r_1)v(|\vec{R}+\vec{r}_2-\vec{r}_1|)\rho(r_2)\,d\vec{r}_1\,d\vec{r}_2\,, \qquad (1)$$

where the coordinates are defined in Fig. 7. Here $\vec{r}_1$ and $\vec{r}_2$ refer to the nucleon coordinates in the target and projectile, respectively, R is the distance between the centers-of-mass of the two ions, ρ is the nucleon density in each nucleus, and v is a prescribed effective nucleon-nucleon interaction. The potential which results might be expected to be a reasonable approximation only for the tail region of the real potential, given the frozen density assumption contained in Eq. (1), above. In those cases of elastic scattering where strong absorption effects prevent any appreciable overlap of the two ions this is sufficient. However, this is not the case for the $^{12}C+^{12}C$ system over the energy region investigated here; nonetheless, the lack of success with the Woods-Saxon real potentials suggested the need for a new approach to a description of the potential.

The densities in Eq. (1) were obtained by generating simple independent particle model wave functions for the $s_{1/2}$ and $p_{3/2}$ nucleons (protons and neutrons were treated separately) using Woods-Saxon well-depth parameters which reproduce experimental nucleon separation energies. The geometries of the wells were adjusted to achieve values for the rms radius (corrected for the finite size of the nucleon) in agreement with recent electron scattering results.[30] The resulting Woods-Saxon potential had parameter values $r_0 = 1.15$ fm, $a = 0.65$ fm, together with a spin-orbit coupling of 17 times the Thomas form, and for the protons, the Coulomb potential from a uniform charge of radius $1.35 \times 11^{1/3}$. The proton separation energies were taken to be 16 MeV ($1p_{3/2}$) and 31 MeV ($1s_{1/2}$), while for the neutrons we used 18.7 MeV ($1p_{3/2}$) and 33.7 MeV ($1s_{5/2}$). These gave rms radii of 2.295 fm (protons) and 2.272 fm (neutrons). Corrections for the center-of-mass recoil[31]

TABLE I. Optical model parameters.

Potential	V (MeV)	W (MeV)	r_V [a] (fm)	a_V (fm)	r_W [a] (fm)	a_W (fm)
A	38–400	6–13	0.9–1.2	0.6–0.9	~1.31	~0.5
B	10–12	5–16	~1.4	~0.3	~1.3	~0.38
C	10–12	~25	~1.35	~0.5	~1.27	~0.25

[a] The potential radius is $R_{V,W} = 2 \times 12^{1/3} \times r_{V,W}$.

were not made; other studies have shown that these have negligible effect on the resulting potential, provided a density distribution with the correct rms radius is used. Since this density is spherical and the interaction v is central, the resulting folded potential $V(R)$ is also spherically symmetric.

The spin-, isospin-independent effective interaction v used in Eq. (1) was taken from the work of Bertsch *et al.*[32]

$$v(r) = -1961 \frac{e^{-2.5r}}{2.5r} + 6315 \frac{e^{-4r}}{4r} - 818(\vec{r}) \text{ MeV}. \quad (2)$$

In this work, the Yukawa terms were obtained[32] by fitting to G-matrix elements for even states in an oscillator basis calculated using the Reid potential. It was assumed that the odd-state interaction was purely a one-pion exchange potential. Some exchange effects are included in Eq. (2) by using a zero-range pseudopotential which mocks up single-nucleon exchange effects.[29,33] A similar calculation using the density-dependent G matrix of Day[34] (also based upon the Reid potential) gives a very similar potential.

The folded potential, together with a Woods-Saxon imaginary potential, was used in the code HIGENOA; the resulting angular distributions were compared with data individually at each energy, with the following parameters subject to variation:

(a) N, the normalization of the folded potential (1), with $N \approx 1$ meaning the folding model is successful,
(b) W, the depth of the imaginary potential, and
(c) r_W and a_W, the radius and diffuseness of the imaginary Woods-Saxon potential, respectively, which were finally fixed at $r_W = 1.22$ fm and $a_W = 0.54$ fm for all energies after an initial global consideration of all angular distributions.

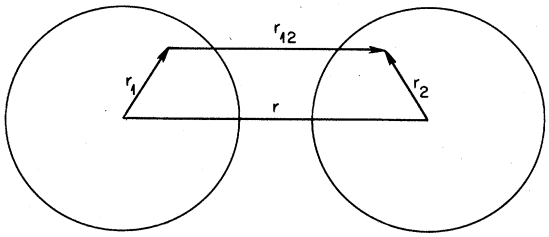

FIG. 7. The coordinates used in the folding integration.

A charge radius parameter $r_c = 1.3$ fm was used for the Coulomb potential.

The results of these two-parameter fits appear in Fig. 3; the corresponding variations of N and W are shown in Fig. 8. It can be seen that all values of N are within ± 5% of an average value having a slight linear energy dependence as shown. Similarly, the change in the depth of the imaginary potential is well reproduced by a linear energy dependence as shown. The sensitivity of the theoretical curves at large angles (Fig. 3) to the magnitude of N can be appreciated by noting that if real potentials with depths given by the straight line in Fig. 8 are used, the general magnitude of the cross sections for the large angles is unaffected, but the phase of the oscillations can change quite drastically. The variations in W have no such effect.

The relative success (i.e., $N \approx 1$) of the folding-model potential appears to be derived from its characteristic shape, quite different from the shape of the Woods-Saxon potential. As shown in Fig. 9, the folding potential is deeper and has a larger slope over the region $r = 0$–6 fm. The parameters of this shallow Woods-Saxon potential

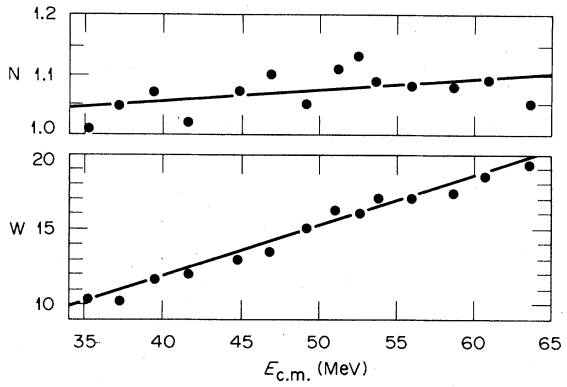

FIG. 8. The values of the normalization factor N for the real, folded potential and the depth W of the imaginary potential which best fit the measured angular distributions at each energy.

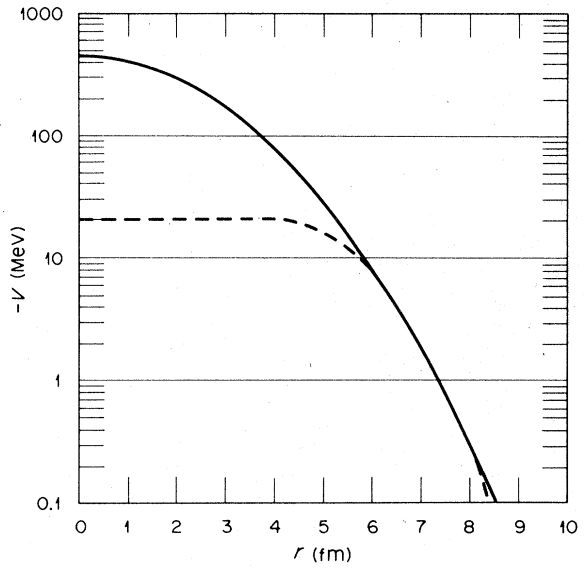

FIG. 9. Comparison of the folding-model real potential and a typical shallow Woods-Saxon potential (V = 20 MeV, r_V = 1.25 fm, a_V = 0.52 fm).

were chosen to fit the forward-angle cross sections at $E_{c.m.}$ = 58.55 MeV (E_{lab} = 117.1 MeV), using the same imaginary Woods-Saxon potential as used with the folded real potential. A comparison of the theoretical results is shown in Fig. 3, where the cross sections predicted by this shallow potential are shown by the dashed curve; these results are characteristic of shallow Woods-Saxon potentials.

It is interesting to note an improved potential shape can also be achieved phenomenologically by using the square of the Woods-Saxon form factor and a corresponding large depth V. This choice results in fits to the data comparable to those obtained with the folded potential. The corresponding potential is then very close in shape to the folded one.[35]

The sensitivity of the optical model results to the interior of the real nuclear potential can be studied in more detail in a number of ways. One of the simplest is to modify the shape of the potential in stages in such a way as to localized any point or region of sensitivity. We have done this by flattening the potential in the region inside some truncated radius R_T, and stepping R_T from R_T = 0 to R_T = 8 fm in steps of 1 fm. The effects of these truncations on the resulting angular distributions at $E_{c.m.}$ = 58.55 MeV are shown in Fig. 10 for several values of R_T. The case R_T = 1 fm gives a result identical to the full (or R_T = 0 fm) potential calculation, but clearly the oscillations in the predicted angular distributions at the backward angles are extremely sensitive to the shape of the real nuclear potential into as far as $r \sim 2$ fm.

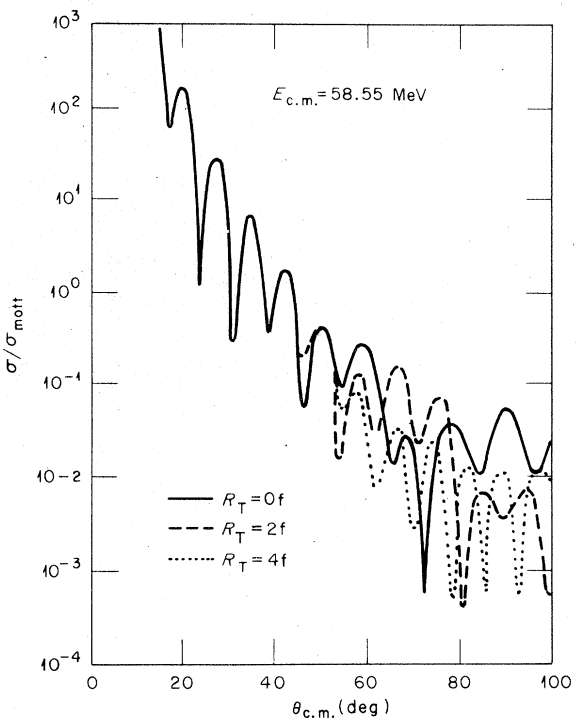

FIG. 10. The effect on the elastic angular distribution at $E_{c.m.}$ = 58.55 MeV of flattening the real, folded potential for $R < R_T$.

To ensure that the discontinuity in slope introduced by the flattening did not introduce spurious reflections which might have distorted the resulting angular distributions, the discontinuities were smoothed with an exponential factor that removed any such possibility. The results were not affected.

The observed sensitivity to the interior region can be further investigated by examining the radial wave functions which result from use of the two potentials shown in Fig. 9 and which result in the angular distributions shown in Fig. 3. Shown in Fig. 11 are the moduli of wave functions generated using the two potentials for the partial waves L = 0, 10, and 18. It is clear that there are appreciable effects on the wave functions for the folded potential in the interior region r = 0–4 fm that do not appear in the Woods-Saxon potential wave functions.

The sensitivity of these wave functions at small-r and low-L values can be seen by noticing that a 10% change in the normalization N of the folding-model potential drastically alters the phase of the wave function over that region as well as upsetting the good fits of the calculated cross sections to the data at the large angles.

Another important aspect which shows the difference in the two potentials is the behavior of the

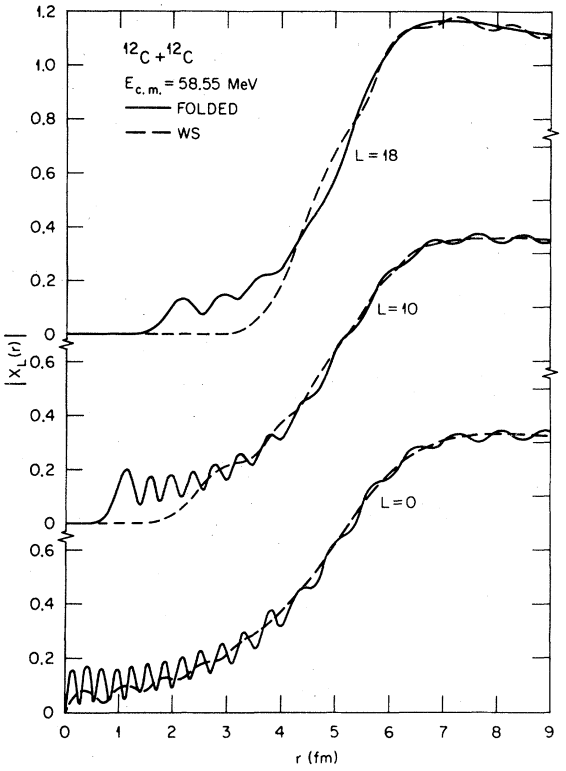

FIG. 11. Comparison of the partial-wave radial functions for the folded real potential and the Woods-Saxon potential shown in Fig. 9.

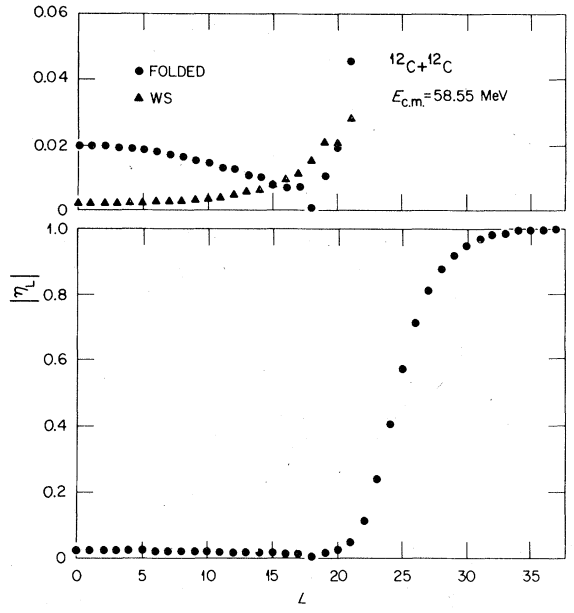

FIG. 12. Comparison of the reflection coefficients (moduli of the scattering-matrix elements) for the folded real potential and the Woods-Saxon potential shown in Fig. 9.

partial-wave scattering-matrix elements η_L. The behavior of $\eta_L = A_L e^{i2\delta_L}$ as a function of L is the same for both potentials when $L > 22$. However, their behavior for the lower partial waves ($L \lesssim 20$) is completely different. The folded-potential scattering matrix shows much more rapid changes in phase than does the one for the Woods-Saxon potential. Figure 12 shows the reflection coefficients or magnitudes $|\eta_L|$ of the scattering-matrix elements at $E_{c.m.} = 58.55$ MeV for both the folded and the Woods-Saxon potentials. The $|\eta_L|$ for $L > 22$ are very similar, but as the expanded scale for the upper half of the figure shows, those for $L < 20$ show appreciable differences. The folded potential shows the characteristics of reflection from the interior contrifugal barrier due to the slight penetration of these low-L partial waves into the interior. The importance of the low partial waves in accounting for certain features of the $^{12}C + ^{12}C$ scattering has been pointed out by Rowley *et al.*[36]

The observed sensitivity of the calculated angular distribution to the interior region of the potential depends vitally on the relatively weak absorption that is presented by the imaginary potential. With the real and imaginary potential used at $E_{lab} = 121.6$ MeV, for instance, the mean free path is ~2 fm. However, all attempts to increase the absorption (by increasing W or by using an imaginary potential with the same shape as the real, folded one) resulted in a marked degradation of the fits to the data. Thus within the context of a local optical model analysis of these data, strong absorption effects cannot be invoked to eliminate the sensitivity to the interior.

The question of the uniqueness of these folded potentials has been studied by Rowley *et al.*[36] for the particular case $E_{lab} = 102.1$ MeV. They modify the real and imaginary potentials with form factors which tend to decrease the potentials at small radii while preserving their shape in the region $r > 4$ fm. An examination of the resulting S-matrix elements indicates the existence of discrete ambiguities in the shape of the potential in the region $r \gtrsim 4$ fm.

We have used their prescription to examine the effects of such modifications on the actual angular distributions. It appears that discrete changes in the potential for $r < 4$ fm, in the way suggested by Rowley *et al.*,[36] can still provide fits to the data which are of comparable quality. Consequently, although the angular distributions are sensitive to the potential in this inner region of 0–4 fm, we are unable to draw any unambiguous conclusions about its strength. However, the present analysis does seem to determine unambiguously the potential at distances in as far as 4 fm. (Modifying the potential at distances larger than 4 fm causes the fits

to deteriorate.) We note that Re $U(r)$ has reached about -80 MeV at $r=4$ fm and has values for $r \simeq 4$ to 6 fm which are substantially stronger than those given by Woods-Saxon potentials derived from fits to data at lower bombarding energies. It is the different shape of the folded (or Woods-Saxon squared) potential in this surface region which is responsible for the improved fits obtained here.

B. Inelastic scattering

1. Coupled-channel effects

Over much of the angular range the inelastic cross sections for single excitation of the 2^+ state at 4.43 MeV are comparable to, or larger than, the elastic cross sections. Even the mutual excitation of both ions to their 2^+ states sometimes has a larger cross section than for elastic scattering. Such a situation often means that the coupling to this excited state is so strong that its effects on the elastic scattering cannot be subsumed in a simple optical model and that the distorted-wave approximation (DWA) is inadequate for calculating the inelastic cross sections. Nonetheless, some earlier coupled-channel calculations[37,38] for this reaction at 126 MeV indicated that the coupling effects were not that strong and that small adjustments in the optical model parameters were all that were needed in order for the simple optical model and the DWA to give a reasonably good account of the data.

The distorted-wave method uses optical potentials which, in general, differ from those in a coupled-channel description because they are adjusted to fit the observed elastic scattering. Thus they include, in a phenomenological way, some of the effects of the coupling to the excited states which are included explicitly in a coupled-channel calculation. Consequently one difficulty in making a comparison between the results of coupled-channel calculations and those using the simple optical model plus the distorted-wave method is that a meaningful comparison requires that both methods give the same elastic scattering. This is difficult to achieve for a system such as $^{12}C+^{12}C$, and indeed such an exact equivalence has not been obtained by us. Consequently, although some exploratory coupled-channel calculations were made[35] for the present data which suggested that explicit effects of coupling to this 2^+ excited state might be important, the question remains open. In addition, coupled-channel calculations are considerably more expensive, so at this time we have not obtained fully satisfactory fits to our data using them. Nevertheless, the calculations which were done gave no reason to believe that our inability to fit the data with shallow Woods-Saxon potentials was a consequence of neglecting coupled-channel effects. Coupled-channel calculations using shallow Woods-Saxon potentials tended to err at large scattering angles in the same manner as the optical model (with a similar potential).

2. Folding model for excitation of the 2^+ state

Following the spirit of the folding model used to describe the elastic scattering, we used the same effective nucleon-nucleon interactions[29,30] of Eq. (2). Surprisingly, the transition density ρ_t for the $0^+ \rightarrow 2^+$ transition has not been well determined. For convenience we chose the Tassie or hydrodynamical model form[39] for the radial dependence of the transition density

$$\rho_t(r) = Cr \frac{df_t}{dr} ,$$

where

$$f_t(r) = \left(1+\exp \frac{r-c_t}{a_t}\right)^{-1} .$$

In principle the radius and diffuseness parameters c_t and a_t should be determined from electron inelastic scattering to this state. (Such measurements allow one to deduce the proton transition density; for this excitation in ^{12}C, it is reasonable to assume that this equals the neutron transition density.) The normalizing constant C is chosen so that ρ_t reproduces the measured $B(E2)$ value. We chose the value[40] $B(E2)\uparrow = 42\ e^2\ \text{fm}^4$. (More recent measurements[41] give an average value of 39 ± 4 e^2 fm.) In the choice of c_t and a_t we were guided by the analysis of electron scattering data.[42] The transition density obtained in that way is reasonably well produced by using $c_t = 1.5$ fm, $a_t = 0.65$ fm. Then we require $C = 0.171$ fm^{-3}. In order to test the sensitivity of the predicted scattering to the details of the density, we also made calculations with $c_t = 2.5$ fm, $a_t = 0.50$ fm (with $C = 0.099$ fm^{-3}), and also $c_t = 1.5$ fm, $a_t = 0.50$ fm (with $C = 0.456$ fm^{-3}).

The resulting transition density is then folded with the density distribution of the ground state of the other ion and the effective interaction Eq. (2) to give the transition potential. Then there are no adjustable parameters. Figure 13 shows the three choices of transition density and the resulting transition potentials $U_t(r)$. Although the densities are significantly different, the potentials are quite similar, especially near $r \approx 6$ fm. In particular, the full and dashed curves are very close, and indeed we find that they yield almost identical cross sections.

It is well known that the coupling potential for inelastic scattering usually has to be chosen com-

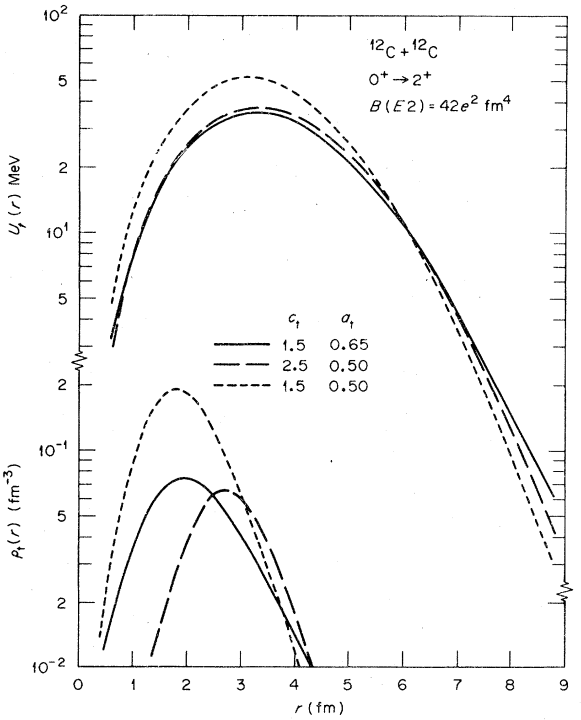

FIG. 13. Transition potentials for three choices of transition density, as calculated using the folding model.

plex in order to reproduce the measurements. When the collective model is used, this is achieved by deforming both real and imaginary parts of the optical potential. There is as yet no satisfactory microscopic theory for the imaginary part of the interaction, so we adopted the usual hybrid approach. The real potential was calculated as just described, but the imaginary part was obtained by deforming the imaginary part of the optical potential in the usual way. A deformation parameter $|\beta_2| = 0.60$ was used, corresponding to $B(E2) = 42$ e^2 fm^4 for a uniform charge distribution of radius $1.2\ A^{1/3}$ fm. Inclusion of this imaginary part of the interaction increases the predicted inelastic cross sections by 30 to 40% in magnitude, with some smaller changes in the angular distributions, and improves the agreement with the data.

Coulomb excitation may be included. It had been found previously[37] that its effects were very small at 126.5 MeV, and we verified that it could also be neglected at 70.7 MeV where it changed the cross sections by at most a few percent. Consequently Coulomb excitation was not included in the calculations now to be reported.

3. *Comparison with the data for single 2^+ excitation*

The inelastic cross sections were calculated by the DWA using the transition potentials just described and the optical potentials with the optimum values of the normalization parameter N and the imaginary strength W obtained by fitting the elastic scattering at each energy (see Fig. 3). (The same values of N and W were used for the transi-

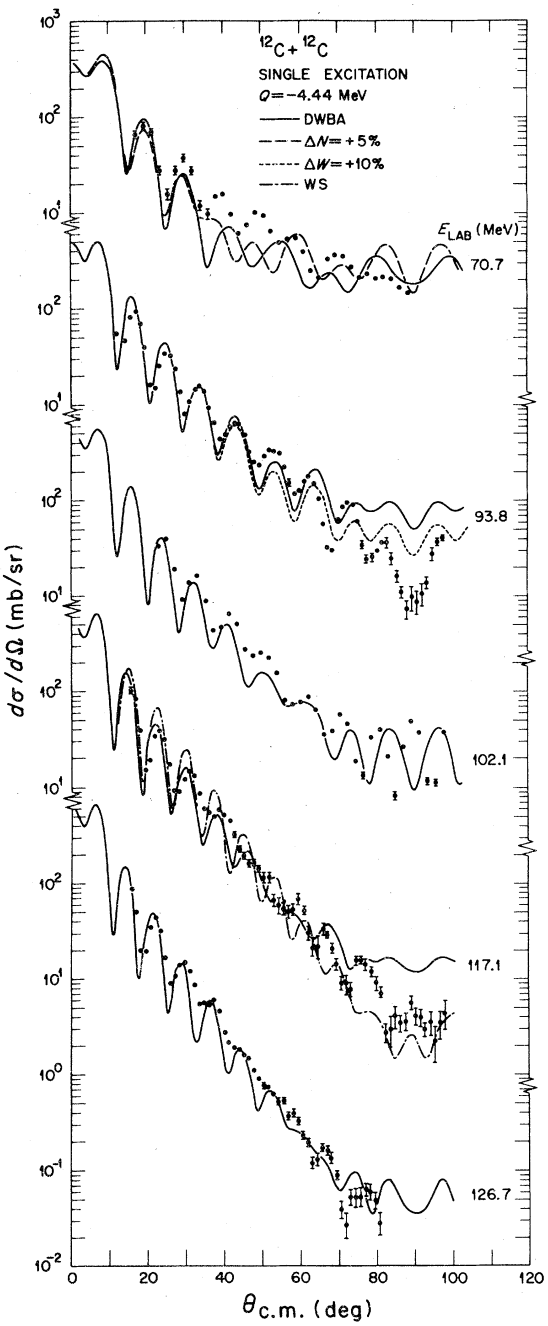

FIG. 14. Comparison of the data with the predicted inelastic cross sections using the folding model. The dashed curve results from increasing the real potential strength by 5%, the dotted curve from increasing the absorptive strength by 10%. The dot-dash curve was calculated using a deformed Woods-Saxon potential.

tion potentials.) This was done at five representative energies. Figure 14 compares these predictions, for the transition density with $c_t = 1.5$, $a_t = 0.65$, with the measured values.

We see that in general the agreement is very satisfactory; no parameter adjustment was allowed, and the absolute magnitude of the cross sections is determined by the $B(E2)$ value adopted. Some of the details of the angular distributions are quite sensitive to small changes in the parameters (just as is the case with the elastic scattering). For example, the angular distribution at the lowest energy, 70.7 MeV, oscillates somewhat out of phase with the measurements, but the results at this energy are somewhat sensitive to the normalization of the real potential. The dashed curve in Fig. 14 shows the effects of increasing this by 5%, from $N = 1.01$ to $N = 1.06$. The structure then agrees better with the data. This result is due to the changes produced in the elastic distorted waves rather than in the transition potential.

Also shown in Fig. 14 are the predictions for 117.1 MeV using the Woods-Saxon potential shown in Fig. 9 (whose elastic cross sections are shown in Fig. 3 and the corresponding wave functions in Fig. 11). The simple collective model was used with the deformation parameter $\beta = 0.60$ for both real and imaginary parts. Somewhat poorer agreement with the data is obtained at this particular energy (except in the immediate vicinity of $\theta \approx 90°$, in contrast with the elastic scattering).

The other transition potentials (see Fig. 13) were also used; that arising from use of $c_t = 2.5$, $a_t = 0.50$ gave almost the same inelastic cross sections. The use of $c_t = 1.5$, $a_t = 0.50$ did produce some changes in the inelastic scattering, increasing the cross sections as one approaches 90°. The effect is larger at the lower energies (over 50% at 90° and 70.7 MeV) than at the higher (about 30% at 126.7 MeV), and causes the agreement with the data to deteriorate.

There are small fluctuations in the optimum values of W at the various energies (see Fig. 8) so calculations were made to see the sensitivity of the inelastic cross sections to these. The dotted curve in Fig. 14 shows the effects at 93.8 MeV of increasing W from 13.5 to 14.7 MeV. The general reduction in cross section, especially at the larger angles, is characteristic of the consequences of increasing W. In this particular case it improves the agreement with the data.

In summary, the use of a transition density suggested by inelastic electron scattering measurements and a known $B(E2)$ value, together with the interaction which reproduces the measured elastic scattering, gives a remarkably good parameter-free account of the single excitation of the 2^+ state at 4.43 MeV. The remaining discrepancies between the theoretical and measured cross sections are of the same order as those found for the elastic scattering and can be attributed to the sensitivity of this light system to small uncertainties in the parameter values and to the details of the reaction mechanisms which may be treated rather crudely by the simple models employed here.

V. DISCUSSION

The scattering of $^{12}C + ^{12}C$ at these energies appears to be sensitive to the optical model potential at distances of separation of the centers-of-mass of the ions as small as ~4 fm and to require this potential to have a shape which is not of the Woods-Saxon form but more like the square of this form. The proper shape and strength are given by the folding model using a realistic interaction.

This is reminiscent of $^{40}Ca + \alpha$ scattering whose "anomalous" behavior at large angles has been well known for some years. It has been shown recently[43] that this behavior can also be explained in detail by the use of a potential whose shape is of the Woods-Saxon form raised to the power 2.65. Such a potential, and the corresponding scattering, are also reproduced closely[44] by a folded potential using the same interaction as used here.

In both cases, the sensitivity to the interior arises because of the unusually weak absorptive potentials that are required. In the case of α particles bombarding the Ca isotopes, the changes in the characteristics of the scattering can be reproduced by changes in the strength of this absorptive potential if the folding model is used for the real potential.[45] This has been interpreted[36,46] as due to interference between waves reflected at the exterior Coulomb barrier and internal centrifugal barrier; as the absorption is increased, the latter becomes of less importance.

This interpretation might seem to imply a surprisingly large probability of finding two ^{12}C nuclei passing through one another and retaining their identities. However, the magnitudes of the reflection coefficients $|\eta_L|$ for the penetrating partial waves are still very small (Fig. 12); this is confirmed by the wave functions in Fig. 11 which show explicitly that this probability is not very large. The transmission coefficients for $L \leq 20$ are $T_L \leq 0.000\,4$ at this energy; one ^{12}C is far from being "transparent" to the other. The magnitudes of these $|\eta_L|$ are similar to those found for fits to the anomalous $^{40}Ca + \alpha$ cases[43-45]; although they are very small compared to unity for the penetrating partial waves, they are still several orders of magnitude larger than those for more typical strongly absorbed situations such as $^{58}Ni + \alpha$ or

$^{40}Ca+^{40}Ca$. The T_L for the Woods-Saxon potential (Figs. 9 and 12) are more like the latter. It appears that only a slight penetration, with interior waves of quite small amplitude, is able to produce the effects seen. It is indeed intriguing that the deep, folded potential obtained from a realistic interaction is just such as to produce this penetration for both the $^{12}C+^{12}C$ and $^{40}Ca+\alpha$ cases. Nonetheless, it remains to be seen whether these interior wave functions correspond to reality or are just an artifact of the model.

It would be of interest in the future to extend the folding-model analyses described here to the reactions of $^{12}C+^{12}C$ at lower energies[14-17] and also to the experimental results available for $^{16}O+^{16}O$ (Ref. 10). In the former case, it must be borne in mind that the contributions of compound elastic scattering increase as the bombarding energy is reduced, thus making it more difficult to draw firm conclusions from a comparison of theory and experiment. Further insight into the physical implications of the potentials which have been found to reproduce the present experimental data could be gained also from a detailed semiclassical analysis, such as has been done by Brink and Takigawa for the case of $\alpha+^{40}Ca$ (Ref. 46). Such analyses provide a quantitative framework for the discussion of phenomena such as shape resonances and orbiting.

This research was sponsored by the Division of Basic Energy Sciences, U. S. Department of Energy, under Contract No. W-7405-eng-26 with the Union Carbide Corporation.

[1]J. S. Blair, in *Lectures in Theoretical Physics*, edited by P. D. Kunz, D. A. Lind, and W. E. Brittin (University of Colorado Press, Boulder, 1966), Vol. VIIIC.
[2]J. A. McIntyre, S. D. Baker, and K. H. Wong, Phys. Rev. 125, 584 (1962).
[3]W. E. Frahn and R. H. Ventner, Ann. Phys. (N.Y.) 24, 243 (1963).
[4]G. Igo, Phys. Rev. Lett. 1, 72 (1958).
[5]G. R. Satchler, in *Proceedings of the International Conference on Reactions between Complex Nuclei, Nashville, Tennessee, 1974,* edited by R. L. Robinson, F. K. McGowan, J. B. Ball and J. H. Hamilton (North-Holland, Amsterdam/American Elsevier, New York, 1974), Vol. 2, p. 171; in Proceedings of the Symposium on Macroscopic Features of Heavy-Ion Collisions, Argonne, Illinois, 1976 (unpublished).
[6]P. J. Moffa, C. B. Dover, and J. P. Vary, Phys. Rev. C 13, 147 (1976).
[7]A. Gobbi, R. Wieland, L. Chua, D. Shapira, and D. A. Bromley, Phys. Rev. C 7, 30 (1973).
[8]A. J. Baltz, P. D. Bond, J. D. Garrett, and S. Kahana, Phys. Rev. C 12, 136 (1975).
[9]R. Siemssen, in *Proceedings of the International Conference on Resonances in Heavy-Ion Reactions*, edited by N. Cindro (North-Holland, Amsterdam, 1977), p. 79.
[10]J. V. Maher, M. W. Sachs, R. H. Siemssen, A. Weidinger, and D. A. Bromley, Phys. Rev. 188, 1665 (1969).
[11]H. J. Fink, W. Scheid, and W. Greiner, Nucl. Phys. A188, 259 (1972).
[12]D. Shapira, R. G. Stokstad, and D. A. Bromley, Phys. Rev. C 10, 1063 (1974).
[13]R. G. Stokstad, in *Proceedings of the International Conference on Reactions between Complex Nuclei, Nashville, Tennessee, 1974,* edited by R. L. Robinson, F. K. McGowan, J. B. Ball, and J. H. Hamilton (North-Holland, Amsterdam/American Elsevier, New York, 1974), Vol. 2, p. 327.
[14]D. A. Bromley, J. A. Kuehner, and E. Almqvist, Phys. Rev. Lett. 4, 365 (1960); E. Almqvist, D. A. Bromley, J. A. Kuehner, and B. Whalen, Phys. Rev. 130, 1140 (1963); H. Spinka and H. Winkler, Nucl. Phys. A233, 456 (1974).
[15]W. Reilly, R. Wieland, A. Gobbi, M. W. Sachs, J. Maher, R. H. Siemssen, D. Mingay, and D. A. Bromley, Nuovo Cimento 13A, 913 (1973); W. Reilly, Ph.D. thesis Yale University, 1972 (unpublished).
[16]R. Wieland, A. Gobbi, L. Chua, M. W. Sachs, D, Shapira, R. Stokstad, and D. A. Bromley, Phys. Rev. C 8, 37 (1973); R. Wieland, Ph.D. thesis, Yale University, 1973 (unpublished).
[17]H. Emling, R. Nowotny, D. Pelte, G. Schrieder, and W. Weidenmeier, Nucl. Phys. A211, 600 (1973); H. Emling, R. Nowotny, D. Pelte, G. Schrieder, and W. Weidenmeier, Nucl. Phys. A239, 172 (1975).
[18]K. H. Wang, S. D. Baker, and J. A. McIntyre, Phys. Rev. 127, 187 (1962).
[19]G. T. Garvey, A. M. Smith, and J. C. Hiebert, Phys. Rev. 130, 2397 (1963).
[20]M. L. Halbert, C. B. Fulmer, S. Raman, M. J. Saltmarsh, A. H. Snell, and P. H. Stelson, Phys. Lett. 51B, 341 (1974).
[21]S. Raman, C. B. Fulmer, M. L. Halbert, M. J. Saltmarsh, A. H. Snell, and P. H. Stelson, in *Proceedings of the International Conference on Reactions between Complex Nuclei, Nashville, Tennessee, 1974,* edited by R. L. Robinson, F. K. McGowan, J. B. Ball, and J. H. Hamilton (North-Holland, Amsterdam/American Elsevier, New York, 1974), Vol. I, p. 2.
[22]R. M. Wieland, R. G. Stokstad, G. R. Satchler, and L. D. Rickertsen, Phys. Rev. Lett. 37, 1458 (1976).
[23]C. B. Fulmer, R. M. Wieland, D. C. Hensley, S. Raman, G. R. Satchler, A. H. Snell, P. H. Stelson, and R. G. Stokstad, Phys. Rev. C 20, 670 (1979).
[24]R. G. Stokstad, R. M. Wieland, C. B. Fulmer, D. C. Hensley, S. Raman, A. H. Snell, and P. H. Stelson, Oak Ridge National Laboratory, Report No. ORNL/TM-5935, 1977, available from the authors or from the National Technical Information Service, U. S. Department of Commerce, 5285 Port Royal Road, Springfield, Virginia 22161. (Note: In this compilation, the absolute values of the cross sections, σ, should be used. The values of σ/σ_{Mott} contain a small normaliza-

tion error in some cases.)
[25]Supplied by Penn Spectra Tech, Philadelphia, Pennsylvania.
[26]HIGENOA, an optical model code written by F. G. Perey and modified by C. Y. Wong and L. W. Owen.
[27]R. A. Chatwin, J. S. Eck, D. Robson, and A. Richter, Phys. Rev. C 1, 795 (1970).
[28]O. Tanimura, Institute for Nuclear Study, University of Tokyo Report No. 267, 1976 (unpublished).
[29]G. R. Satchler and W. G. Love, Phys. Lett. 65B, 415 (1976); and to be published.
[30]C. W. DeJager, H. DeVries, and C. DeVries, At. Data Nucl. Data Tables 14, 479 (1974).
[31]C. M. Shakin and V. Weiss, Phys. Rev. C 15, 1911 (1977).
[32]G. Bertsch, J. Bonysowicz, H. McManus, and W. G. Love, Nucl. Phys. A284, 399 (1977).
[33]W. G. Love and L. W. Owen, Nucl. Phys. A239, 74 (1975).
[34]Y. Eisen and B. Day, Phys. Lett. 63B, 253 (1976).
[35]L. D. Rickertsen, G. R. Satchler, R. G. Stokstad, and R. M. Wieland, in Proceedings of the Symposium on Macroscopic Features of Heavy-Ion Collisions, Argonne, Illinois, 1976, Vol. II, Argonne National Laboratory Report No. ANL-PHY-76-2, 1976 (unpublished).
[36]N. Rowley, H. Doubre, and C. Marty, Phys. Lett. 69B, 147 (1977).
[37]R. H. Bassel, G. R. Satchler, and R. M. Drisko, in *Proceedings of the Third International Conference on Reactions between Complex Nuclei, Asilomar, 1963*, edited by A. Ghiorso, R. M. Diamond, and H. E. Conzett (University of California Press, Berkeley, 1963); Nucl. Phys. 89, 419 (1966).
[38]N. Austern and J. S. Blair, Ann. Phys. (N.Y.) 33, 15 (1965).
[39]H. Uberall, *Electron Scattering from Complex Nuclei* (Academic, New York, 1971).
[40]R. H. Stelson and L. Grodzins, Nucl. Data 1A, 1 (1965).
[41]F. Ajzenberg-Selove, Nucl. Phys. A248, 1 (1976).
[42]R. M. Haybron, M. B. Johnson, and R. J. Metzger, Phys. Rev. 156, 1136 (1967).
[43]F. Michel and R. Vanderpooten, Phys. Rev. C 16, 142 (1977).
[44]W. G. Love, Phys. Rev. C 17, 1876 (1978).
[45]F. Michel, Phys. Rev. C 13, 1446 (1976); G. R. Satchler (unpublished).
[46]N. Austern, Ann. Phys. (N.Y.) 15, 299 (1961); G. R. Satchler and R. H. Bassel, Phys. Lett. 5, 347 (1963); D. M. Brink and N. Takigawa, Nucl. Phys. A279, 159 (1977).